Coverage dependence of magnetic domain structure and magnetic anisotropy in supported Fe nanoparticles on Al_2O_3/NiAl(100)

Wen-Chin Lin,[1,a)] C. B. Wu,[2] P. J. Hsu,[2] H. Y. Yen,[2] Zheng Gai,[3] Lan Gao,[3] Jian Shen,[3] and Minn-Tsong Lin[2,4]
[1]*Department of Physics, National Taiwan Normal University, 11677 Taipei, Taiwan*
[2]*Department of Physics, National Taiwan University, 10617 Taipei, Taiwan*
[3]*Center for Nanophase Materials Science Division, Oak Ridge National Laboratory, Oak Ridge, Tennessee 37831, USA and Materials Science and Technology Division, Oak Ridge National Laboratory, Oak Ridge, Tennessee 37831, USA*
[4]*Institute of Atomic and Molecular Sciences, Academia Sinica, 10617 Taipei, Taiwan*

(Received 22 January 2010; accepted 1 June 2010; published online 6 August 2010)

Studies of magnetic domain and magnetic anisotropy in collected nanoparticles are crucial for both understanding interparticle interaction and engineering in applications. In order to characterize the microscopic surface morphology and the nanoscale magnetic domain structure of Fe nanoparticles, a scanning tunneling microscope and a scanning electron microscope with polarization analysis (SEMPA) were used in our experiment. For the coverage of 9–13 monolayers (MLs) Fe deposited on Al_2O_3/NiAl(100), circular and well-separated nanoparticles were grown. As the coverage increased up to 23–33 ML, these Fe nanoparticles started to coalesce and form elongated islands. Therefore a transition from isotropic to anisotropic in-plane magnetism was observed. Our proposed uniaxial magnetic anisotropy models effectively explain the azimuthal angle dependent two-step hysteresis loops. Moreover, the *in situ* measured SEMPA images clearly show the coverage dependent evolution of magnetic domain structure. Variations in interparticle interaction and magnetic correlation length with increasing Fe coverage are also reported. © *2010 American Institute of Physics*. [doi:10.1063/1.3457794]

I. INTRODUCTION

Due to symmetry breaking at the surface and the high ratio of surface/bulk atomic numbers, magnetic nanostructures are expected to reveal unique and controllable properties.[1,2] Many studies have been reported on the theoretical simulation and experimental characterization of various magnetic nanoparticles. In theoretical simulations, several models have been proposed to describe the influence of dipolar interaction, multipole interaction, tunneling exchange coupling, etc.[3–7] The magnetic anisotropy and domain structure of collected nanoparticles can be engineered by controlling particle size and interdistance, so that nanoparticle assemblies provide more tunable properties and may replace conventional thin films.[8–10]

The microscopic magnetic behavior of nanoparticles is particularly crucial for developing future applications. For example, in nanodevices or memory storage devices, microscopic magnetic behavior is strongly correlated with the functionalities of nanoscale local areas.[11–16] Thus this study considers the following questions. How do magnetic properties, including the collective hysteresis loops and the microscopic magnetic domain structure, change with increasing coverage, which reduces the interparticle gaps until coalescence? Dose the coalesced nanoparticle assembly behave like isolated particles or a continuous thin film? It is noteworthy that surface contamination is another crucial factor in experiments, since the gaps between nanoparticles are usually of atomic scale. Ultrahigh vacuum (UHV) *in situ* fabrication and measurement are thus particularly important to explore these essential issues. In our experiment, Fe nanoparicles were grown on a self-organized single-crystalline Al_2O_3 layer. With increasing Fe coverage, the nanoparticles became lager, gradually leading to the coalescence of nearby nanoparticles and the formation of elongated islands.

For determining the magnetic characteristics, macroscopic measurements are usually carried out by averaging techniques such as the magneto optical Kerr effect (MOKE), or the superconducting quantum interference device. Studies based on microscopic imaging are generally performed with scanning probe techniques such as spin-polarized scanning tunneling microscopy (SP-STM) (Refs. 17 and 18) and magnetic force microscopy,[19–22] which are generally difficult to use for imaging nanoparticles due to the interference of the morphological corrugations. In contrast, scanning electron microscopy with polarization analysis (SEMPA) is less affected by morphology and gives a vector signal that is directly proportional to the magnetization.[23] Therefore, measurements of UHV-MOKE, SEMPA, and STM were combined in our experiment, providing the best spatial resolution for the imaging of morphology and spin contrast.[23] In our previous study, the magnetic coupling between separated particles was characterized quantitatively,[10] whereas this report is more focused on the coverage dependence of the magnetic behavior. A transition from isotropic in-plane magnetization to anisotropic in-plane magnetism is observed when Fe coverage is increased from 13 to 23 monolayers (MLs).

[a)]Electronic mail: wclin@ntnu.edu.tw.

Based on a statistical analysis of nanoscale magnetic domain images, the particle–particle magnetic coupling and the coalescence effect are analyzed.

II. EXPERIMENT

All experimental processes, including sample preparation, transferring, and measurement were performed in UHV chambers with the base pressure better than 2×10^{-10} mbar. After cycles of Ar^+ sputtering and annealing, the Al_2O_3/NiAl(100) template was prepared by high-temperature oxidation of the NiAl(100) substrate at 1000 K.[24] Then Fe nanoparticles were grown by evaporation onto the Al_2O_3/NiAl(100) template at room temperature (RT). The nominal thickness of Fe nanoparticles is expressed in units of MLs, which is defined as the atomic density on a Cu(100) surface of 1.54×10^{15} at./cm^2, since the deposition rate was calibrated from the epitaxial growth on Cu(100). The morphology of Fe nanoparticles was ascertained by a scanning tunneling microscope (STM).[25] The collective magnetic behavior was investigated by the MOKE at RT.[26] A scanning electron microscope with spin analysis (SEMPA) was used to study the magnetic domain structure of the as-grown Fe nanoparticle assemblies at RT. The SEMPA was equipped with a spin polarized low energy electron diffraction detector, which measured the spin contrast in two orthogonal directions simultaneously during the scanning. Thus the in-plane magnetization vectors at each pixel of a SEMPA image can be determined.

III. RESULT AND DISCUSSION

A. Growth of Fe nanoparticle assemblies

As shown in Fig. 1, high temperature oxidation of NiAl(100) provides a single-crystalline Al_2O_3 layer as the template for self-organized nanopatterning. In Fig. 1(a), the Al_2O_3 domain size ranges over hundreds of nanometer. As seen in the more detailed image of Fig. 1(b), the Al_2O_3 domains are composed of Al_2O_3 stripes along the ⟨010⟩ and ⟨001⟩ directions, with an interdistance of ~4 nm and stripe length in the tens to hundreds of nanaometer.[27] The length and width of the rectangular Al_2O_3 domains are determined directly from the STM images. The length-width plot and size distribution are plotted in Figs. 1(c)–1(e). The Al_2O_3 domains are strongly correlated with the magnetic domains, particularly after particle coalescence. This correlation is discussed later in the text.

Similar to our previous report on Co nanoparticles,[24,25,28] the initial growth of Fe nanoparticles shows a self-limiting size distribution, and is directed by domain boundaries or linear stripes of the single crystalline Al_2O_3 surface, forming regular one-dimensional particle chains. As the coverage increases, the particle size increases and the one-dimensional ordering gradually disappears. Figure 2 shows the STM images of 9–33 ML Fe nanoparticle assemblies on Al_2O_3/NiAl(100). The measurements of particle density, size distribution, and length/width ratio are summarized in Fig. 3. The size of each particle is determined by the full width at half maximum (FWHM) of its cross-section. Length

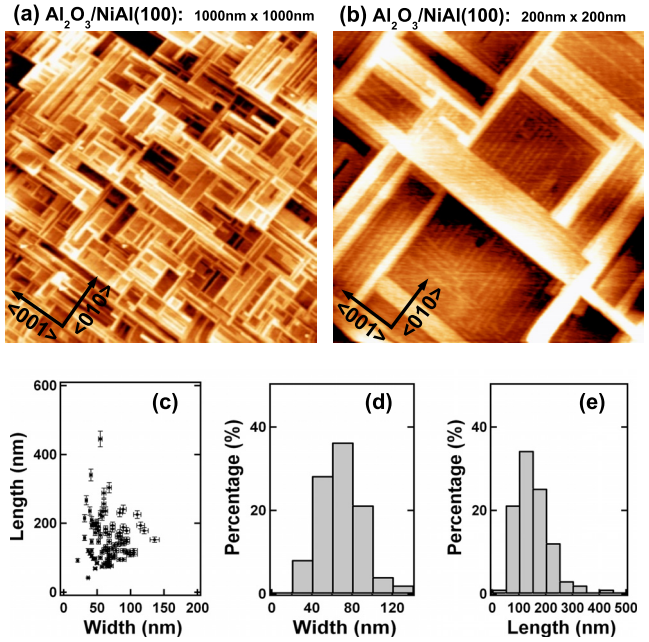

FIG. 1. (Color online) (a) STM image of Al_2O_3/NiAl(100) template of large scale. The surface is composed of rectangular Al_2O_3 domains. (b) Magnified STM image of Al_2O_3/NiAl(100) template revealing that the Al_2O_3 domains are constructed from ~4 nm wide nanostripes. (c) Length-width plot of Al_2O_3 domains. [(d) and (e)] Width and length distribution of Al_2O_3 domains.

and width are defined as the measured FWHM distances from the longest and shortest cross-sections, respectively. The particle density decreases with increasing coverage. For 9 ML Fe, the particles are isolated and of circular shape (length/width ratio ~1) with diameter ~3–8 nm. The particle size distribution is confined by the Al_2O_3 stripes (interdistance ~4 nm), resulting in a high probability at particle width of 4 nm. Increasing the coverage to 13 ML [see Fig. 3(c)] dose not significantly increase the FWHM of the size distribution. Very large particles (>10 nm) are seldom seen. The gaps between nanoparticles are observable, and they

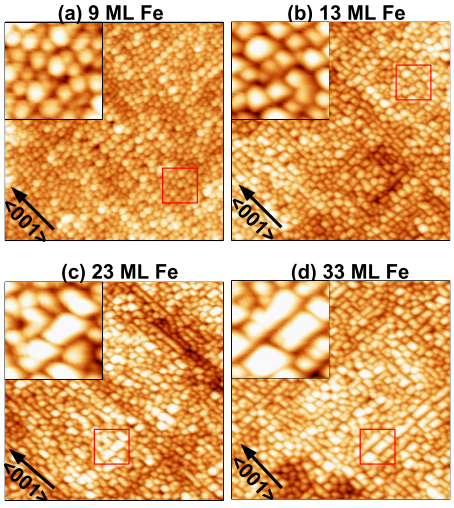

FIG. 2. (Color online) STM images (250×250 nm^2) of (a) 9 ML, (b) 13 ML, (c) 23 ML, and (d) 33 ML Fe nanoparticle assemblies on Al_2O_3/NiAl(100). The insets show the magnified images of the areas (40×40 nm^2) indicated by squares.

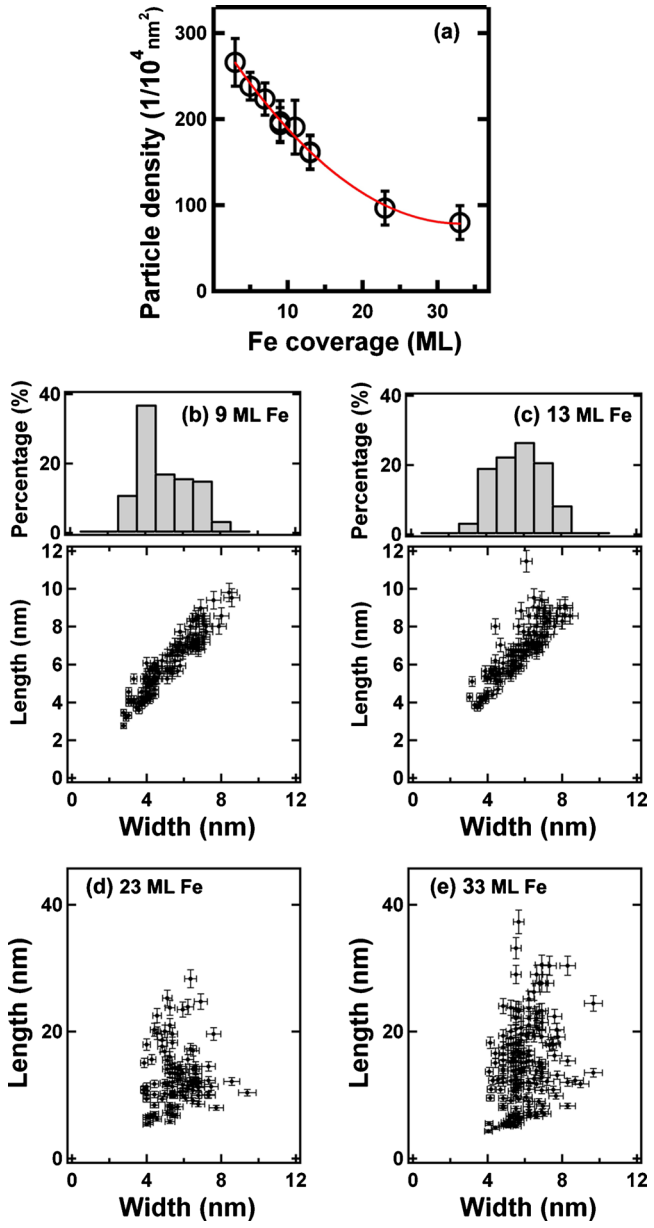

FIG. 3. (Color online) Statistics of Fe nanoparticle assemblies. (a) Nanoparticle density as a function of Fe coverage. [(b) and (c)] The particle width distributions and the length/width plots of 9 and 13 ML Fe nanoparticles. [(d) and (e)] The length/width plots of 23 and 33 ML Fe nanoparticles.

maintain their circular shape. With the higher coverage of 23–33 ML Fe, the particles coalesce to form elongated islands along the stripes of the Al_2O_3 template. As indicated in Figs. 2(c) and 2(d) and Figs. 3(d) and 3(e), the lengths of elongated islands range from 10 to 25 nm and from 10 to 40 nm for 23 ML and 33 ML, respectively, while the width is still within 3–8 nm. The coalescence effect on magnetism, especially the magnetic anisotropy, is discussed later.

B. MOKE measurement

9–33 ML Fe nanoparticle assemblies prepared in this experiment reveal in-plane magnetic anisotropy, without any observable hysteresis loops in the surface-normal direction.[28] The in-plane Kerr remanence measured at RT is summarized as a function of Fe coverage in Fig. 4(a). The zero Kerr

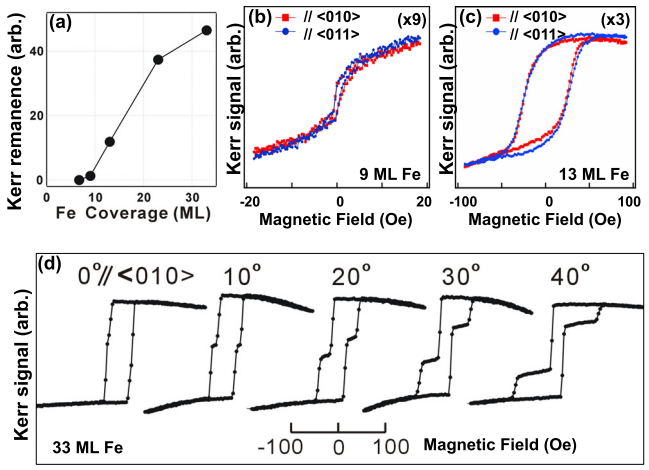

FIG. 4. (Color online) (a) Kerr remanence of n ML Fe deposited on Al_2O_3/NiAl(100) recorded at RT. [(b)–(d)] In-plane MOKE hysteresis loops of 9, 13, and 33 ML Fe nanoparticle assemblies, measured at different azimuthal angles.

remanence at 8 ML indicates that the Curie temperature (T_c) of 8 ML Fe nanoparticles is below RT or the magnetic relaxation time at RT is faster than the MOKE measurement time scale (a few seconds). The significant reduction in the magnetic long-range exchange coupling in Fe nanoparticle assembly, indicated by the reduced Curie temperature (T_C) or blocking temperature (T_B), as compared with the thin films, is consistent with the fact that the nanoparticles are still separated.[28]

Above 9 ML the in-plane hysteresis loops become observable. The Kerr remanence gradually increases with Fe coverage. Figure 4 exhibits the in-plane MOKE hysteresis loops recorded at RT. For 9 ML Fe, the ratio of remanence/saturation is less than 50%, as shown in Fig. 4(b). The hysteresis loops measured with the applied field along ⟨010⟩ and ⟨011⟩ appear similar, indicating that there is no preferred easy axis in the surface plane. This is reasonable since the shape of nanoparticles is isotropic in the surface plane and the particle alignment seems insignificant. The 13 ML Fe nanoparticle assembly also reveals isotropic hysteresis loops. The ratio of remanence/saturation increases to ~75%. For 33 ML Fe, as shown in Fig. 4(d), the in-plane MOKE hysteresis loop reveals two steps when the azimuthal angle ϕ differs from zero.

From the two-step hysteresis loops displayed by 23–33 ML Fe/Al_2O_3/NiAl(100) with azimuthal ϕ rotation, we summarize the coercivity field (H_C) as a function of azimuthal angle ϕ, relative to ⟨010⟩ in Fig. 5. H_{C1} and H_{C2} are defined as the coercivity of the first and second magnetization switching in the two-step loops, as indicated in the inset of Fig. 5. H_{C1} increases with ϕ and reaches two to three times the initial value when ϕ is close to 45°. Inversely, H_{C2} decreases with increasing ϕ and becomes nearly half the initial value when ϕ is near 45°.

Similar two-step hysteresis loops (double magnetic switching) have been previously reported in various systems, such as follows: (1) ferromagnetic bilayer in which one layer is of soft magnetism and the other is of hard magnetism;[29] (2) stepped surface in which surface steps induce a uniaxial

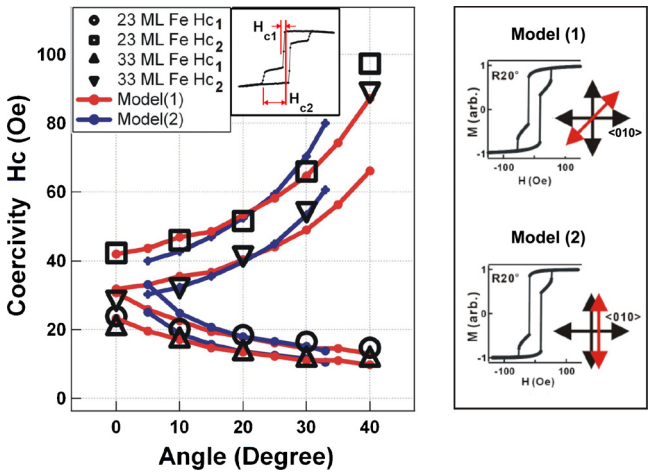

FIG. 5. (Color online) Angle dependence of H_{C1} and H_{C2} with fitting results. The inset shows the definition of H_{C1} and H_{C2} in the two-step MOKE hysteresis loops. The right panel reveals simulated hysteresis loops for 20° rotated sample in models (1) and (2). The black and red arrows indicate the directions of the fourfold and uniaxial anisotropy, respectively, in the models.

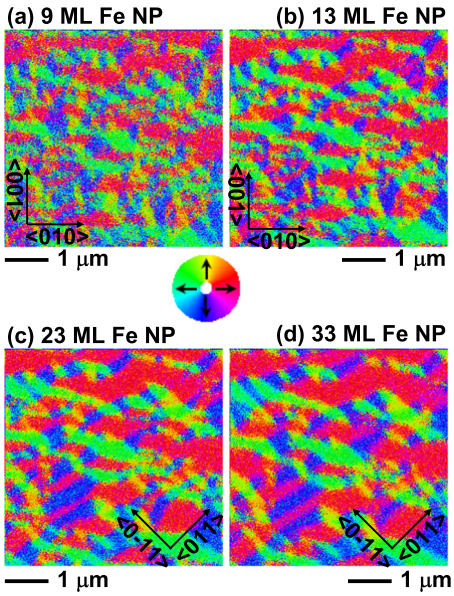

FIG. 6. (Color online) SEMPA images of as-grown 9–33 ML Fe nanoparticle assemblies at the same position after sequential deposition. The different colors indicate the magnetization directions.

anisotropy;[30,31] (3) ring magnet in which the two steps are related to the onion state and vortex state;[32] (4) ferromagnetism/antiferromagnetism (FM/AFM) systems;[33,34] and (5) nanodots with perpendicular magnetization.[35,36] Although our experimental system does not fully fit with any of the above prereported conditions, we can also try to use ideas from the literature to propose some possible explanations for our experimental results. Generally the "two-step" hysteresis loop is due to some metastable states which occur during the magnetization switching. Therefore the biaxial crystalline anisotropy is usually combined with a uniaxial or unidirectional anisotropy term in the Stoner–Wohlfarth model for simulating two-step loops.[31,33,34] The uniaxial anisotropy can be induced by surface steps or lattice mismatch. The unidirectional anisotropy is caused by FM/AFM coupling, which is not the case in our experiment. Thus we try to combine a biaxial anisotropy with a uniaxial anisotropy to simulate the azimuthal angle dependent magnetic behavior, as shown in Figs. 4 and 5. The energy E of this system is given by

$$E = -H \cdot M \cos(\phi - \theta) + K_1 \sin^2(2\theta) + K_2 \sin^2(\theta - \delta). \quad (1)$$

The first term in Eq. (1) is the Zeeman energy. θ and ϕ are the rotation angles of the magnetic moment and magnetic field, respectively, relative to ⟨010⟩. K_1 is the fourfold magnetic anisotropy preferring ±⟨010⟩ and ±⟨001⟩ directions. K_2 is the uniaxial magnetic anisotropy along the δ angle relative to ⟨010⟩. Minimizing the total energy E allows the M-H hysteresis loops to be plotted with different azimuthal angle ϕ. Then we try to find if any conditions leads to two-step loops. After considering the symmetry of our sample and trying various values of K_1, K_2, and δ, we find the two conditions, δ=45° and 90°, in which the two-step hysteresis loops appear when $0° \leq \phi \leq 45°$. Thus the uniaxial magnetic anisotropy prefers ⟨011⟩ and ⟨001⟩ directions, which we refer to as the δ=45° model(1) and the δ=90° model(2), respectively. For the two conditions δ=45° and 90°, we set the anisotropy energies, K_1 and K_2, as free parameters, and try to fit the experimental results of H_{C1} and H_{C2}. K_1 and K_2 are tuned independently in the two models. Eventually, the best fit for both models gives nearly the same values of K_1 and K_2. With $K_1 = 1.4 \pm 0.2$ and $K_2 = 2.1 \pm 0.4$ μeV/atom, the simulation result is very close to the measured angle-dependent H_{C1} and H_{C2}, as shown in Fig. 5(c). Small deviations of K_1 and K_2 (0.2–0.4 geV/atom) do not change the simulation results very much. Actually $K_1 = 1.4 \pm 0.2$ and $K_2 = 2.1 \pm 0.4$ μeV/atom are close to the magnetic anisotropy of bulk Fe which is 3.56 μeV/atom.[37] The consistency also supports the rationality and validity of our model simulation.

From the above discussion, we conclude that a uniaxial anisotropy appears after coalescence. The averaged deviation between the simulation and the experimental data is 9% and 15% (normalized by experimental data) for model(1) and model(2), respectively. From this, model(1) seems to fit our experimental data better, especially in the range $0° \leq \phi \leq 30°$. The lattice match between the Al_2O_3 template and the 45°-rotated Fe body-center-cubic crystalline might be the cause for the δ=45° uniaxial anisotropy in model(1). This proposed reason is very different from the conventional step-induced or exchange bias-induced uniaxial anisotropy in previously published works.[29,30,32,33]

C. Magnetic domain structure

Figure 6 shows SEMPA images of as-grown 9–33 ML Fe nanoparticle assemblies at the same position after sequential deposition. The different colors indicate the magnetization directions. With increasing coverage, many fine structures merge into large domains. Especially, the frustrated or unstable domain configurations evolve into flux closure (vortex-like) magnetic domains. The magnetic domains consist of many vortex-like structures, as indicated by the circles in Fig. 7(a), with the vortex size around several hundreds of

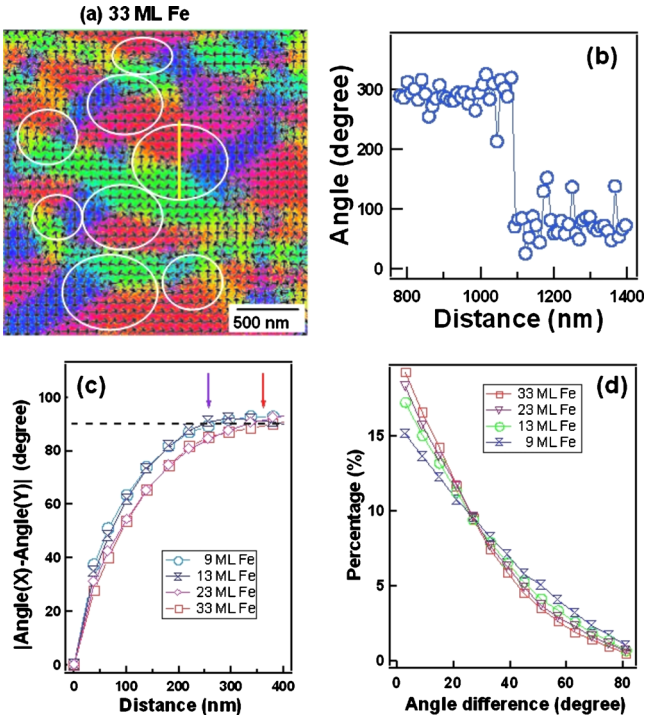

FIG. 7. (Color online) (a) Magnified SEMPA image of 33 ML Fe nanoparticles. The arrows indicate the magnetization directions. The white circles mark the flux closure magnetic domain structures. (b) Line profile of the magnetization direction, as indicated in (a). The magnetization switches within 10 nm, about the size of a single nanoparticle. (c) The correlation functions of 9–33 ML Fe nanoparticles. The arrows indicate the magnetic correlation length to be ~250 and 350 nm for 9–13 and 23–33 ML Fe nanoparticles, respectively. (d) Histogram of angle differences between nearby pixels (pixel size: 10×10 nm^2) in SEMPA images of 9–33 ML Fe nanoparticles.

nm. As shown in Fig. 7(b), magnetization switching is observed within one pixel (10 nm) at the center of the vortexes.

From the SEMPA images, the correlation function, which is defined as the averaged magnetization angle difference, $|\mathrm{Angle(X)}-\mathrm{Angle(Y)}|$, can be calculated as a function of distance for each pair of pixels X and Y. The averaged angle difference between two uncorrelated pixels should be ~90°, which is the average of random distribution between 0° and 180°. Therefore we can determine the effective length of magnetic coupling by finding when dose the correlation function approach 90°. The correlation functions of magnetic directions of Fe nanoparticle assemblies are summarized in Fig. 7(c). The magnetic correlation length is deduced to be ~250 and 350 nm for 9–13 ML and 23–33 ML Fe, respectively. The 250 to 350 nm correlation length is at least two to three orders of magnitude smaller than the domain size of in-plane magnetized thin films, which is typically in the range from hundreds of micrometer to millimeter.[10,38] The much smaller domain size observed in the Fe nanoparticle assembly is likely to be caused by the reduced magnetic coupling and anisotropy energy, which lead to lower energy cost for creating domain walls.

As shown in Fig. 6, the magnetic domains of 23–33 ML Fe are over 250–350 nm in length. However, length of the elongated Fe islands ranges only 20–40 nm, as shown in Fig. 2. The following questions rise. Why is the extent of the magnetic domain much larger than the size of Fe islands? What is the correlation between the magnetic domain and the elongated islands? Actually, the magnetic domain size is of the same order of the Al_2O_3 domain size, as shown in Fig. 1(a). Fe nanoparticles grown on the same Al_2O_3 domain (terrace) reveal collective magnetic behaviors. The magnetic interaction across different Al_2O_3 domains is relatively weak, probably due to the different domain height or larger interparticle gaps at the domain boundary. The higher Fe coverage increases the particle height and induces coalescence between particles, promoting the magnetic interaction between different Al_2O_3 domains and resulting in the extension of magnetic domains. Although the coalescence induced elongated Fe islands do not correspond directly to the magnetic domain shape or size, they still change the collective magnetic anisotropy, leading to the two-step hysteresis loops. Possible mechanisms include the coalescence induced shape, crystalline, or interface related magnetic anisotropy.

Furthermore, the statistics for magnetization angle difference $\Delta\theta$ between nearby pixels is analyzed in order to study the magnetic coupling strength between the nearest neighbor pixels. Figure 7(d) summarizes the distribution of $\Delta\theta$ between the nearest neighbor of pixels. Apparently the nearest neighbors prefer parallel alignment ($\Delta\theta=0$), and the coupling strength increases monotonically with the Fe coverage. These results are obvious. With higher deposition coverage, the particle size increases and the interparticle gap gets smaller. Thus we observe a clear increase in coupling strength, indicating the possibility of controlling the magnetic coupling strength and magnetic anisotropy for the desired magnetic properties, such as magnetic correlation length, Curie temperature, and domain configuration, through tunable particle size, interdistance, or alignment.[9,25]

In the magnified SEMPA images, such as Fig. 7(a), the pixel size is 10×10 nm^2. The pixel size is very close to the average interparticle distance of the circular nanoparticles in 9–13 ML Fe, as shown in Fig. 1. Thus, as reported in our previous paper,[10] the coupling energy E can be obtained by fitting the experimental $\Delta\theta$ distribution [Fig. 7(d)] with a simplified magnetic coupling model. The fitted curves describe the statistical distribution well. The fitted coupling energy E is 79 ± 2 meV and 98 ± 3 meV for the 9 ML and 13 ML Fe nanoparticles, respectively, which is very close to the dipolar coupling energy (~94 meV) between two Fe nanodiscs with diameter of 10 nm, center-to-center distance of 10 nm and height of 2 nm.[5,20,39] Thus it is possible that the dipolar interaction is an origin for the extended domain structures of Fe nanoparticle assemblies.

Up to now, many theoretical simulations[22,39] and experiments[20,22] have investigated the magnetic properties of nanoparticle assemblies, especially for the reduced magnetic correlation length and the flux closure (vortex-like) magnetic domain structures. In the study of Scheinfein *et al.* by neutron scattering, the magnetic correlation length of Fe nanoparticle assemblies ranges from 100 to 120 nm for 10–15 nm in diameter.[40] Monte Carlo simulations of Bennett *et al.*[39] and Georgescu *et al.*[22] show that the magnetic moments of nanoparticles arrange themselves into flux closure structures. The vortex state is determined to be the most stable condition, with the nanoparticles close to each other and coupled

by dipolar interaction. Although the simulation has been reported, it is still difficult to observe a real image due to the limitation of investigative tools. Therefore, instead of performing a similar simulation, we emphasize that the *in situ* direct observation by SEMPA, in Figs. 6 and 7, indeed provides conclusive evidence to support the aforementioned simulation.

IV. SUMMARY

By combining *in situ* MOKE, STM, and SEMPA investigations, we have studied the coverage dependence of macroscopic and microscopic characteristics of Fe nanoparticle assemblies, including particle shape evolution, size distribution, magnetic hysteresis loop, magnetic flux-closure domain structure, magnetic correlation length, and magnetic coupling strength. For 9–13 ML Fe, the isolated circular nanoparticles revealed isotropic ferromagnetism on the surface plane. For 23–33 ML Fe, coalesced particles formed elongated islands along the stripes of Al_2O_3 template, revealing anisotropic in-plane magnetization. It is concluded that a uniaxial magnetic anisotropy explains the transition from isotropic to anisotropic in-plane magnetization. In the microscopic magnetic domain structure, when the Fe coverage was increased from 9–13 ML to 23–33 ML, the coalescence of nanoparticles extended the magnetic correlation length from 250 to 350 nm, which is two to three orders of magnitude smaller than the domain size of continuous thin films. From a statistical analysis of SEMPA images, the dipolar interaction between Fe nanoparticles was determined to play a dominant role in the formation of both the extended magnetic domain structures and the vortex-like domains. These conclusions will be valuable for engineering magnetic nanoparticle assemblies for designed functionalities.

ACKNOWLEDGMENTS

This work was supported by the National Science Council of Taiwan under Grant Nos. NSC 96-2120-M-002-011, NSC 95-2112-M-002-051-MY3, and NSC 96-2112-M-003-015-MY3. A portion of this research at Oak Ridge National Laboratory's Center for Nanophase Materials Sciences was sponsored by the Scientific User Facilities Division, Office of Basic Energy Sciences, U.S. Department of Energy.

[1]F. J. Himpsel, J. E. Ortega, G. J. Mankey, and R. F. Willis, Adv. Phys. **47**, 511 (1998).
[2]D. K. Singh, R. Krotkov, and M. T. Tuominen, Phys. Rev. B **79**, 184409 (2009).
[3]S. A. Majetich and M. Sachan, J. Phys. D: Appl. Phys. **39**, R407 (2006).
[4]E. Y. Vedmedenko, N. Mikuszeit, H. P. Oepen, and R. Wiesendanger, Phys. Rev. Lett. **95**, 207202 (2005).
[5]P. Poddar, T. Telem-Shafir, T. Fried, and G. Markovich, Phys. Rev. B **66**, 060403(R) (2002).
[6]O. Petracic, A. Glatz, and W. Kleemann, Phys. Rev. B **70**, 214432 (2004).
[7]M. A. K. Zilani, Y. Y. Sun, H. Xu, Y. P. Feng, X.-S. Wang, and A. T. S. Wee, Phys. Rev. B **72**, 193402 (2005).
[8]M. R. Scheinfein, K. E. Schmidt, K. R. Heim, and G. G. Hembree, Phys. Rev. Lett. **76**, 1541 (1996).
[9]S. Tomita, K. Akamatsu, H. Shinkai, S. Ikeda, H. Nawafune, C. Mitsumata, T. Kashiwagi, and M. Hagiwara, Phys. Rev. B **71**, 180414(R) (2005).
[10]W. C. Lin, Z. Gai, L. Gao, J. Shen, P. J. Hsu, H. Y. Yen, and M.-T. Lin, Phys. Rev. B **80**, 024407 (2009).
[11]H.-J. Freund, Surf. Sci. **500**, 271 (2002).
[12]M. Bäumer, M. Frank, M. Heemeier, R. Kühnemuth, S. Stempel, and H.-J. Freund, Surf. Sci. **454–456**, 957 (2000).
[13]M. Heemeier, S. Stempel, S. K. Shaikhutdinov, J. Libuda M. Bäumer, R. J. Oldman, S. D. Jackson, and H.-J. Freund, Surf. Sci. **523**, 103 (2003).
[14]S. G. Grancharov, H. Zeng, S. Sun, S. X. Wang, S. O'Brien, C. B. Murray, J. R. Kirtley, and G. A. Held, J. Phys. Chem. B **109**, 13030 (2005).
[15]J. Xie, S. Peng, N. Brower, N. Pourmand, S. X. Wang, and S. Sun, Pure Appl. Chem. **78**, 1003 (2006).
[16]S. Sun, H. Zeng, D. B. Robinson, S. Raoux, P. M. Rice, S. X. Wang, and G. Li, J. Am. Chem. Soc. **126**, 273 (2004).
[17]U. Schlickum, W. Wulfhekel, and J. Kirschner, Appl. Phys. Lett. **83**, 2016 (2003).
[18]A. Kubetzka, O. Pietzsch, M. Bode, and R. Wiesendanger, Phys. Rev. B **63**, 140407(R) (2001).
[19]V. F. Puntes, P. Gorostiza, D. M. Aruguete, N. G. Bastus, and A. P. Alivisatos, Nature Mater. **3**, 263 (2004).
[20]M. Georgescu, J. L. Viota, M. Klokkenburg, B. H. Erné, D. Vanmaekelbergh, and P. A. Zeijlmans van Emmichoven, Phys. Rev. B **77**, 024423 (2008).
[21]S. A. Koch, R. H. Te Velde, G. Palasantzas, and J. T. M. De Hosson, Appl. Phys. Lett. **84**, 556 (2004).
[22]M. Georgescu, M. Klokkenburg, B. H. Erné, P. Liljeroth, D. Vanmaekelbergh, and P. A. Zeijlmans van Emmichoven, Phys. Rev. B **73**, 184415 (2006).
[23]H. P. Oepen and J. Kirschner, Scanning Microsc. **5**, 1 (1991).
[24]W. C. Lin, C. C. Kuo, M. F. Luo, K.-J. Song, and M.-T. Lin, Appl. Phys. Lett. **86**, 043105 (2005).
[25]W. C. Lin, S. S. Wong, P. C. Huang, C. B. Wu, B. R. Xu, C. T. Chiang, H. Y. Yen, and M.-T. Lin, Appl. Phys. Lett. **89**, 153111 (2006).
[26]W. C. Lin, C. C. Kuo, C. L. Chiu, and M.-T. Lin, Surf. Sci. **478**, 9 (2001).
[27]P. J. Hsu, C. B. Wu, H. Y. Yen, S. S. Wong, W. C. Lin, and M.-T. Lin, Appl. Phys. Lett. **93**, 143104 (2008).
[28]W. C. Lin, P. C. Huang, K.-J. Song, and M.-T. Lin, Appl. Phys. Lett. **88**, 153117 (2006).
[29]B. Rodmacq, V. Baltz, and B. Dieny, Phys. Rev. B **73**, 092405 (2006).
[30]H. C. Mireles and J. L. Erskine, Phys. Rev. Lett. **87**, 037201 (2001).
[31]F. Bisio, R. Moroni, F. Buatier de Mongeot, M. Canepa, and L. Mattera, Phys. Rev. Lett. **96**, 057204 (2006).
[32]J. Rothman M. Kläui, L. Lopez-Diaz, C. A. F. Vaz, A. Bleloch, J. A. C. Bland, Z. Cui, and R. Speaks, Phys. Rev. Lett. **86**, 1098 (2001).
[33]Z.-H. Wang, G. Cristiani, H.-U. Habermeier, and J. A. C. Bland, Phys. Rev. B **72**, 054407 (2005).
[34]C.-H. Lai, Y.-H. Wang, C.-R. Chang, J.-S. Yang, and Y. D. Yao, Phys. Rev. B **64**, 094420 (2001).
[35]A. Bollero, V. Baltz, B. Rodmacq, B. Dieny, S. Landis, and J. Sort, Appl. Phys. Lett. **89**, 152502 (2006).
[36]C.-R. Chang, J. Appl. Phys. **69**, 2431 (1991).
[37]J. P. Pierce, M. A. Torija, Z. Gai, J. Shi, T. C. Schulthess, G. A. Farnan, J. F. Wendelken, E. W. Plummer, and J. Shen, Phys. Rev. B **92**, 237201 (2004).
[38]R. P. Cowburn, J. Ferre, S. J. Gray, and J. A. C. Bland, Phys. Rev. B **58**, 11507 (1998).
[39]A. J. Bennett and J. M. Xu, Appl. Phys. Lett. **82**, 2503 (2003).
[40]J. F. Löffler, H.-B. Braun, and W. Wagner, Phys. Rev. Lett. **85**, 1990 (2000).